Published in final edited form as:
Dev Cell. 2012 September 11; 23(3): 482–493. doi:10.1016/j.devcel.2012.07.009.

Radial construction of an arterial wall

Daniel M. Greif[1,2,3,*], **Maya Kumar**[1], **Janet K. Lighthouse**[3], **Justine Hum**[1], **Andrew An**[1], **Ling Ding**[3], **Kristy Red-Horse**[4], **F. Hernan Espinoza**[1], **Lorin Olson**[5], **Stefan Offermanns**[6], and **Mark A. Krasnow**[1,*]

[1]Department of Biochemistry, Howard Hughes Medical Institute, Stanford University School of Medicine, Stanford, CA 94305, USA

[2]Cardiovascular Division, Department of Medicine, Stanford University School of Medicine, Stanford, CA 94305, USA

[3]Cardiovascular Section, Department of Internal Medicine, Yale University School of Medicine, New Haven, CT 06511, USA

[4]Department of Biology, Stanford University, Stanford, CA 94305, USA

[5]Immunobiology & Cancer Research Program, Oklahoma Medical Research Foundation, Oklahoma City, OK 73104, USA

[6]Max-Planck-Institute for Heart and Lung Research, Dept. of Pharmacology, Ludwigstr. 43, 61231 Bad Nauheim, Germany

SUMMARY

Some of the most serious diseases involve altered size and structure of the arterial wall. Elucidating how arterial walls are built could aid understanding of these diseases, but little is known about how concentric layers of muscle cells and the outer adventitial layer are assembled and patterned around endothelial tubes. Using histochemical, clonal, and genetic analysis in mice, here we show that the pulmonary artery wall is constructed radially, from the inside out, by two separate but coordinated processes. One is sequential induction of successive cell layers from surrounding mesenchyme. The other is controlled invasion of outer layers by inner layer cells through developmentally-regulated cell reorientation and radial migration. We propose that a radial signal gradient controls these processes and provide evidence that PDGF-B and at least one other signal contribute. Modulation of such radial signaling pathways may underlie vessel-specific differences and pathological changes in arterial wall size and structure.

INTRODUCTION

Although there has been remarkable progress over the past decade elucidating the cellular and molecular mechanisms of the critical early events in blood vessel development, generation of new endothelial tubes by vasculogenesis and angiogenesis (Adams and

*Authors for correspondence: daniel.greif@yale.edu, 203-737-2040 (phone), 203-737- 6118 (FAX); krasnow@stanford.edu, 650-723-7191(phone), 650-723-6783 (FAX).

SUPPLEMENTARY INFORMATION
Supplementary information accompanies the paper.

Alitalo, 2007; Carmeliet, 2005; Jin et al., 2005; Phng and Gerhardt, 2009; Strilic et al., 2009; Weinstein and Lawson, 2002), relatively little is known about the subsequent events that create and pattern the arterial wall (Greif, in press; Hungerford and Little, 1999; Hungerford et al., 1996; Schwartz, 1997). A mature arterial wall typically consists of an endothelial monolayer surrounded by multiple concentric rings of smooth muscle cells (SMCs), up to a few dozen or more layers, which dominate the mature arterial wall and provide it with structural integrity and contractility, plus an outer adventitial layer consisting of fibroblasts embedded in a collagen matrix. In many arteries there are also structural specializations such as an elastic layer separating the endothelial cells (ECs) from the vascular smooth muscle cells (VSMCs), and elastic fibers embedded in the smooth muscle layer and other cellular and molecular features that structurally subdivide and pattern the smooth muscle compartment (tunica media) (Frid et al., 1997; Frid et al., 1994; McLean et al., 2005; Wolinsky and Glagov, 1967). The size and pattern of the smooth muscle layer are carefully controlled in a vessel-specific manner during development, but are dysregulated in many prominent cardiovascular diseases such as aortic aneurysm, coronary artery atherosclerosis and pulmonary hypertension.

Current models of arterial wall development posit that nascent endothelial tubes recruit SMC progenitors, which can apparently arise from a variety of sources (DeRuiter et al., 1997; Esner et al., 2006; High et al., 2007; Jiang et al., 2000; Le Lievre and Le Douarin, 1975; Majesky, 2007; Morimoto et al., 2010; Que et al., 2008; Wasteson et al., 2008; Wilm et al., 2005; Yamashita et al., 2000) and induce them to differentiate into VSMCs. Several signaling pathways have been implicated in VSMC migration or differentiation (Domenga et al., 2004; Gaengel et al., 2009; Hirschi et al., 1998; Lindahl et al., 1997; Mizugishi et al., 2005; Owens et al., 2004; Suri et al., 1996), but how these cells are recruited and organized into a radially-patterned structure with the appropriate number and identity of layers is not well understood. Here we describe the development of the pulmonary artery (PA) wall using histochemical, clonal, and genetic analysis in mice. We show that the wall is constructed radially, from the inside out, by sequential induction and recruitment of successive cell layers from surrounding mesenchymal cells, and by developmentally-regulated invasion of outer layers by inner layer cells. We also show that the endothelial-specific ligand PDGF-B can initiate wall formation but provide genetic evidence that one or more other, as yet unidentified, signals also contribute to the initiation and radial patterning of the wall.

RESULTS AND DISCUSSION

Pulmonary artery smooth muscle cells arise from lung mesenchyme

To elucidate the cellular and molecular events of arterial wall formation, we focused on a small region of a developing mouse artery, the left PA between the level of the carina (ca) and first branch off the left bronchus (LL1; Fig. 1A). We selected this artery because of its relatively simple structure at birth, just two and occasionally three SMC layers plus an outer adventitial layer (Figs. 1B–D), the ease and precision in its identification and developmental staging provided by the adjacent bronchial airways whose full branching program is known (Metzger et al., 2008), and its involvement in devastating diseases such as pulmonary hypertension.

We carried out lineage tracing with cell- and tissue-specific Cre transgenes to investigate the developmental origin of PA SMCs. Previous studies have shown that SMCs of the outflow tract of the right heart originate at least in part from neural crest (Kirby et al., 1983; Majesky, 2007), but SMCs of more distal segments of the PA have been proposed to arise largely from lung mesothelial cells (Que et al., 2008) and ECs (Morimoto et al., 2010) by epithelial- and endothelial-to-mesenchymal transitions. However, our analysis of PA SMCs in E18.5 lungs following lineage tracing with *Wilm's tumor 1* (*Wt1)*-

CreER^{T2}(mesothelium), *VE-cadherin-Cre* (endothelium), *Wnt1-Cre* (neural crest) and *Sonic hedgehog-Cre* (epithelium) transgenes in conjunction with the *ROSA26R^{mTmG}* Cre reporter showed that mesothelium, endothelium, neural crest, and airway epithelium are not substantial sources of SMCs of the PA during this period (Figs. 1E, S1A, B and data not shown). By contrast, lineage tracing with a new lung mesenchyme-specific conditional transgene *Tbx4-CreER^{T2}* (M.K., P. Bogard and M.A.K in preparation and (Menke et al., 2008)), induced at E10.5, resulted in substantial labeling of E18.5 PA cells expressing the SMC marker alpha-smooth muscle actin (SMA), demonstrating that Tbx4^{+} lung mesenchyme is a major, and possibly the sole source of PA SMCs at this stage (Figs. 1F, S1C).

Induction of the first layer of arterial smooth muscle

At ~E11, the first layer of the PA wall begins to form by a stereotyped sequence of molecular and cellular events that occur in the mesenchymal cells surrounding the nascent PA endothelial tube (Fig. 2). Platelet-derived growth factor receptor (PDGFR)-β is initially expressed diffusely in the proximal lung mesenchyme (Fig. 1G), when pulmonary ECs form a widely distributed plexus ((Parera et al., 2005) and P. Bogard, M.K., R. Metzger and M.A.K. in preparation; Fig 1H). But during the next day its expression begins to restrict to the group of mesenchymal cells surrounding the nascent PA endothelial tube, in the domain that will form the arterial wall (Figs. 1I, I′, I″) (see below).

Beginning at ~E11.5, smooth muscle markers such as SMA are induced in the PDGFR-β^{+} cells directly contacting the PA EC tube (Figs. 2A, B). SMA is initially expressed at low levels and in a discontinuous fashion along the length of the PA, with more expressing cells on the lateral than the medial aspect of the vessel and localization of SMA protein initially polarized toward the side of the cell contacting the EC layer (Fig. S2A, B, B′). Other SMC markers also initiate expression at this time including smooth muscle myosin heavy chain (SMMHC) (Miano et al., 1994), the actin and tropomyosin binding protein SM22-alpha, and the transmembrane protein neuron glial-2 (NG2) (Fig. S2F and data not shown). The expression of all four of these SMC markers increases over the next few days, forming a robustly-labeled layer of smooth muscle (Figs. 2C–F, S2C and data not shown).

As SMC markers are induced in first layer cells, PDGFR-β expression is down-regulated in these cells (Fig. S2C) and by E18.5, expression was generally not detected in them (Fig. S2D). Permanent marking of early PDGFR-β-expressing cells with a *PDGFR-β-Cre* transgene (Foo et al., 2006) (Fig. S1E) labeled almost all SMA^{+} PA wall cells at E18.5 (Figs. 1J, S1D), including inner layer cells that do not express PDGFR-β at this time, confirming their origin from cells that initially expressed the gene.

During this period of dynamic marker expression, first layer cells reorient. Initially, at E11.5, many first layer SMA^{+} cells and their nuclei were elongated longitudinally along the blood vessel (Fig. 2A, B, “alignment”). However, over the next few days, first layer cells shortened along their longitudinal axis (Figs. 2C, D, “shortening”), and by E14.5 they were circumferentially oriented (Figs. 2E, F, S2E, “reorientation”), as they are in the mature vessel. Thus, over a three day period (E11.5 to E14.5), the first layer of the PA wall forms by a stereotyped series of cell marker and morphogenesis events.

Sequential induction of the outer layers of the arterial wall

A few days after first layer cells initiate the arterial wall program, surrounding mesenchymal cells initiate a similar series of events to form the second layer of the arterial wall. At E13.5, these second layer cells express PDGFR-β and are elongated longitudinally, as first layer cells were two days earlier (Figs. 2C, D). The next day smooth muscle markers begin to be

expressed in these cells (Figs. 2E, F), and as smooth muscle marker expression increases over the next several days, these cells down-regulate PDGFR-β expression (Fig. S2D), similar to the changes noted in first layer cells several days earlier. During this time, most of the cells shorten in the longitudinal axis and reorient to a circumferential orientation, forming the second layer of the arterial wall (Figs. 1B, C, 2G, H).

As the second layer is forming, cells surrounding this layer initiate a similar program to form the outer layer of the arterial wall. At ~E14, these outer layer cells express PDGFR-β and are elongated longitudinally along the artery (Figs. 2C, D), like early first and second layer cells. However, the outer layer cells do not progress through the full program. By E18.5, they have not turned on SMC markers or down-regulated PDGFR-β expression, and they have not undergone longitudinal shortening or reorientation (Figs. 1B, C, 2G, H). Thus, outer layer cells initiate the arterial wall program but arrest early on, forming the adventitial layer of the wall. These cells do not appear to complete the program, at least not during embryogenesis.

Taken together, the results show that the PA wall is constructed radially, from the inside-out, by sequential activation of an arterial wall program in three successive cell layers.

Radial patterning of cell division in the arterial wall

We next investigated cell division in the developing arterial wall by immunostaining for the mitotic marker phosphohistone H3 (pH3). There were two unexpected results. First, although undifferentiated progenitor cells are thought, in general, to become less proliferative as they differentiate into VSMCs (Owens et al., 2004), we found just the opposite in the developing PA wall. The vast majority of $pH3^+$ mitotic cells (Fig. 3A) of the E11.5–14.5 PA wall are found in the inner (Fig. 3B), more differentiated layers (Fig. 3C), most in the innermost layer directly contacting the endothelial tube (layer 1). Cells that turn on SMA maintain their proliferative index, whereas the proliferative index of cells that do not declines (Fig. 3D).

Second, we found that proliferating inner layer cells undergo a developmental shift in division plane orientation. In the early stages of PA wall development (E11.5–13.5), the axis of division of cells in the inner layer (L1) was predominately (>75%) longitudinal (Figs. 3E, F). However, at E14.5 the axis shifts so that most (~75%) inner layer cells now divide radially (Figs. 3E, F). This shift is specific to the innermost layer: cells in layer two (L2) and the adventitia (A) divide exclusively longitudinally at this stage (Fig. 3F). Below we show by clonal analysis that this shift in division plane orientation corresponds with a transition of inner layer cells to a radially-invasive mode in which they enter and help populate the surrounding cell layer.

Clonal analysis of inner layer cells reveals a transition to a radially-invasive growth mode

A clonal analysis was carried out in which individual first layer SMCs were genetically marked to track their proliferative potential and the final positions and pattern of the daughter cells (Fig. 4A). To label first layer cells with GFP, Cre-mediated recombination was induced in transgenic *SMMHC-creER^{T2}*, *ROSA26R$^{mTmG/+}$* embryos using a single limiting dose (0.8–1.2 mg) of tamoxifen at E11.5, a stage at which SMMHC is expressed exclusively in the first layer of the developing PA wall. This resulted in rare or no GFP^+ cells within the entire visualized region of the left PA, so that labeled cells likely derived from a single recombination event. The putative PA wall clones were scored only if among *SMMHC-creER^{T2}*, *ROSA26R$^{mTmG/+}$* littermates, there was at least one embryo without marked cells in this region. Similar experiments using a multi-color *Rainbow Cre* reporter *ROSA26R$^{Rb/+}$* (Red-Horse et al., 2010) showed that all labeled cells in individual left PAs

were almost always of a single color, confirming their clonal relationship (see Methods). From an analysis of the size of clones between E13.5 and E18.5, we estimate the proliferation rate (doubling time) of PA SMCs as 1.0±0.4 days from E12 to E14, slowing to ~3.8±1.9 days from E14 to E18 (Table S1). (In comparison to these experiments with limiting doses of tamoxifen, a single high dose of tamoxifen labeled substantially more inner layer cells and formed multi-colored “polyclones”, as expected (Figs. S3A–C).)

The positions of daughter cells in 32 PA wall clones derived from individual inner layer cells marked with a limiting dose of tamoxifen at E11.5 and observed at E13.5–18.5 are given in Figure S4 and Table S1. Daughter cells could potentially distribute in longitudinal, circumferential, and radial directions, and the cells could remain contiguous and form a coherent clone or intermingle with unmarked cells to form a dispersed clone (Fig. 4A). At E13.5, marked cells have proliferated and many daughters have migrated extensively along the longitudinal and circumferential axes, often separating from sibling cells and intermixing with unlabeled cells (Figs. 4B, C, E, S4). All the daughter cells, however, remain within the inner, SMA^+ cell layer. A day later, at E14.5, this restriction to radial migration is relaxed, and daughter cells begin to invade the second layer (Figs. 4E, S3D, E, S4). Only a small percentage (12.5%) of marked first layer cells (n=56) have invaded the second layer at E14.5, increasing to 32% by E17.5–18.5 with marked daughter cells found throughout the first and second layers (Figs. 4D, E, S4 and data not shown). The relaxation of the radial restriction is only partial: although marked inner layer cells migrated extensively in the first and second layers, they did not invade the developing adventitial or intimal layers at this stage (Fig. S4). Because there is a full (albeit immature) second layer at E14.5 (Figs. 2E, F), we infer that most second layer cells arise from induction of surrounding (i.e., second layer or beyond) lung mesenchyme (see lineage analysis, Figs. 1F, J, S1C), rather than radial movement of inner layer cells.

A classical clonal analysis of the abdominal aortic wall in adult women using X chromosome-inactivation (analyzed by PCR) as a crude clone marker suggested limited dispersal of sibling cells in most clones (Chung et al., 1998; Schwartz and Murry, 1998), in contrast to the extensive cell migration and mixing we observe. It will be important to revisit this study using high resolution clone markers to determine if this difference represents a fundamental difference between the vessels, organisms, or stages of development, or a limitation of the earlier clone marking and analysis strategy.

A gradient model for radial patterning of the pulmonary artery wall

Our results show that the PA wall is constructed radially, from the inside out (Fig. 5A), by two separate but coordinated processes. One is sequential induction and recruitment of successive cell layers from surrounding mesenchymal progenitor cells. Each layer of mesenchymal cells initiates a program of gene expression and undergoes a stereotyped sequence of morphogenesis events over a three day period; as one muscle layer forms, the next layer initiates development. The program arrests early in the formation of the outermost layer to generate the adventitial layer. The other process is controlled invasion of the surrounding layer by inner layer cells, which initially divide and migrate extensively within the layer but later radially reorient and either migrate into the second layer or radially divide and send daughter cells into the next developing layer. Because this transition to radial invasion coincides with the switch from circumferential to primarily radial cell division, it could be that inner cells only enter an outer layer by radial cell division. Such coupling of centrifugal movement to cell division would prevent depletion of first layer cells, while supplying extra cells needed in the outer layers given their greater circumference but paradoxical dearth of proliferating cells.

We propose that a radial signaling gradient controls and coordinates the two processes (Fig. 5B). The likely source of the signal is the endothelium, and the kinetics of its production and spread, and sensitivity thresholds in the responding mesenchymal cells, would dictate arterial wall identity, the sequence in which these identities arise and the pattern of cell division. Mesenchymal cells directly adjacent to the endothelium, exposed to the highest level of signal, would be the first to induce the smooth muscle program and would proliferate most. As the signal spreads, surrounding mesenchymal cells would initiate the program and begin forming the next layer. The accumulating gradient would also polarize inner layer cells and radially reorient cell division and migration to promote invasion of the surrounding cell layer. The low level of signal received by the outermost mesenchymal cells would be sufficient to initiate but not complete the smooth muscle program, creating the adventitial layer.

PDGF-B is one of multiple radial patterning signals

The ligand PDGF-B is an attractive candidate for the radial patterning signal. It has been implicated in VSMC and pericyte (vascular wall cells associated with capillaries) development (Andrae et al., 2008; Hoch and Soriano, 2003; Lindahl et al., 1997), and it is expressed in ECs of the developing PA starting at the time the arterial wall begins to form (Fig. 5C and data not shown). Its receptors PDGFR-α and PDGFR-β are expressed in an overlapping pattern, complementary to that of PDGF-B, in the surrounding mesenchyme of the early lung (Figs. 1G, I, S5A). When PDGF-B-loaded agarose beads were implanted in E12 embryonic lung cultures, a nascent arterial wall up to two layers thick of PDGFR-β^+, SMA^+ cells began to form around the bead (Figs. 5D–F, S5E-G). Many of these cells were not in direct contact with the bead, suggesting that PDGF-B diffuses away from the bead, forming a local gradient that induces nearby mesenchymal cells to initiate arterial wall formation. Later steps in the arterial wall program, such as downregulation of PDGFR-β expression, did not occur, perhaps because of a requirement for additional signals or declining viability of the explant.

Despite the appropriate expression patterns of PDGF-B and its receptors during arterial wall formation and the ability of PDGF-B to initiate PA wall formation in explants, we found that radial patterning of the PA in mutant embryos null for *PDGF-B* was indistinguishable from that in wild type embryos (Figs. 5G–I). Similar results were obtained for *PDGFR-α*$^{(-/-)}$or *PDGFR-β*$^{(-/-)}$ mutants or conditional *PDGFR-β* gain of function mutants (Figs. 5J, K, S5B-D and data not shown). However, an early step in the process was inhibited in double mutants lacking both PDGF receptors in lung mesenchyme (*PDGFR-α*$^{(flox/-)}$, *PDGFR-β*$^{(-/-)}$, *Tbx4-Cre*) (Figs. 5L, M). Taken together, results of these genetic experiments and the PDGF-B bead experiments implicate PDGF involvement in radial patterning but indicate redundancy among both the ligands and receptors.

Although it would be elegant if the radial patterning signal was a single diffusible factor, our results suggest it is an ensemble of factors, including PDGF-B and at least one other as yet unidentified signal. Multiple factors would provide flexibility in the control of vessel wall structure, important in generating the diversity of such structures and disease phenotypes (see below). And, although it is simplest to think of the factors as diffusible like PDGF-B from the beads, certain features of the process (e.g., the temporal aspect of radial SMC differentiation patterning) could be accounted for by membrane-bound signals transmitted radially via a sequential, contact-dependent (“bucket brigade”) signaling process (Feng et al., 2010; Hoglund and Majesky, 2012; Manderfield et al., 2012).

Implications of the radial patterning model for arterial diversity and disease

Other blood vessels have different radial structures than the PA. For example, at the end of gestation, the left common carotid artery (CCA) and aorta have two or three times the number of smooth muscle layers as the PA, whereas the left anterior descending coronary artery has just a single layer (Figs. 1B, C, 6A-D and data not shown). An analysis of SMA expression and fate mapping of the developing left CCA showed that, as for the PA, the CCA wall forms radially from the inside-out (Figs. 6F–J) with inner layer cells migrating radially to contribute to outer layers (Fig. 6K, L). An initial clonal analysis of the descending thoracic aorta indicates that, here too, inner layer cells migrate radially to contribute to outer layers (A. Misra, L.D. and D.M.G, unpublished data). Thus, despite their differing radial structures, at least some of the same cellular mechanisms are used to form them.

An appealing idea is that vessel-specific modulation of the radial patterning signal(s) and response thresholds generate the observed differences in vessel wall sizes and structures (Fig. 6E), and we further speculate that dysregulation of such signaling contributes to the many vascular diseases in which the radial structure of the vessel wall is altered and SMCs become highly proliferative and motile (Owens et al., 2004), resembling the developmental state (Fig. 6O). Indeed, conditional activation of *PDGFR-β*, which presumably extends and levels the PDGF signaling gradient, markedly increases the thickness of the aorta ((Olson and Soriano, 2011) and Figs. 6M, N), and targeted deletion of the PDGF-B matrix retention motif also alters vessel walls (Lindblom et al., 2003; Nystrom et al., 2006). It must now be a priority to identify the full set of signals that control induction of cell layers and radial invasion, and how generally these pathways and cellular mechanisms operate in development and diseases of each arterial wall. Such pathways and mechanisms would be appealing therapeutic targets for arterial wall diseases and regenerative strategies.

EXPERIMENTAL PROCEDURES

Animals

CD1 mice (Charles Rivers Laboratories) were used for wild type analysis. *PDGF-B*$^{(+/-)}$ (Leveen et al., 1994), *PDGFR-α*^{GFP} (Hamilton et al., 2003), *PDGFR-β*$^{(+/-)}$ (Soriano, 1994), *PDGFR-β-Cre*(Foo et al., 2006), *SMMHC-CreER*^{T2}(Wirth et al., 2008), Rainbow (Rb) Cre reporter *ROSA26R*^{Rb}(Red-Horse et al., 2010), and *PDGFR-β*^{J} (Olson and Soriano, 2011) mice have been described. *PDGFR-α*^{flox}, *Ptch1*^{lacZ}, *Wt1-CreER*^{T2}, *VE-cadherin-Cre, Wnt1-cre, Shh-Cre, SM22-Cre* and the Cre reporter strains *ROSA26R*^{lacZ}, *ROSA26R*^{YFP} and *ROSA26R*^{mTmG} were obtained from Jackson Laboratories. The *Tbx4-Cre* and *Tbx4-CreER*^{T2} transgenes are lung mesenchyme-specific and induce expression of Cre reporters beginning at E10 and throughout the undifferentiated mesenchyme as well as in mesenchymal derivatives, including airway and vascular SMC, but not in airway epithelium (M.K., P. Bogard and M.A.K, in preparation, and (Menke et al., 2008)); construction and use of the transgenes and transgenic mice will be detailed elsewhere (M.K., P. Bogard and M.A.K in preparation).

Immunohistochemistry and histology

Embryos and lungs from timed pregnancies, in which noon of the day of vaginal plug detection was designated E0.5, were dissected and fixed in 4% paraformaldehyde (PFA) for 0.5 – 2 h. For haematoxylin and eosin (H&E) staining, fixed tissue was dehydrated in methanol, and paraffin sections were prepared and stained using standard protocols. For β-galactosidase activity stains, fixed whole mount lungs were incubated with bromo-chloro-indolyl-galactopyranoside (X-gal, Sigma). For immunostains of whole mount lungs (Metzger et al., 2008), fixed lungs were dehydrated serially into 100% methanol and stored

at −20 °C. Lungs were rehydrated and incubated with blocking solution (5% rabbit or goat serum, 0.5% Triton X-100 in PBS) and then with primary antibodies diluted in blocking solution overnight at 4 °C. On the next day, lungs were washed with blocking solution, followed by incubation with fluorescent-conjugated secondary antibodies overnight at 4 °C. For signal amplification, a biotin-conjugated antibody was substituted, and then lungs were incubated with the ABC Elite reagent (Vector) and FITC, Cy3 or Cy5 Tyramide Reagent (Perkin Elmer). For immunostains of cryosections (Red-Horse et al., 2010), fixed tissue was cryoprotected in 30% sucrose overnight at 4 °C, frozen in optical cutting temperature compound (OCT, Tissue Tek) and stored at −80 °C. Tissue was sectioned (10 – 20 μm), washed in PBS and immunostained as described above for whole mount lungs, except sections were incubated with secondary antibodies at room temperature for 1 h.

Primary antibodies used were anti-CD31 (rat 1:100–200, BD Pharmingen; or hamster 1:100, Serotec), anti-VE-cadherin (1:100, BD Pharmingen), anti-E-cadherin (1:500–1000, Invitrogen), anti-NG2 (1:200, Millipore), anti-SMMHC (1:100, Biomedical Technologies), anti-SM22-alpha (1:500, Abcam), anti-PDGFR-α (1:50, R&D), anti-GFP (1:500, Abcam), anti-phosphohistone H3 (pH3; 1:100–200, Millipore), anti-acetylated tubulin (1:500, Sigma), anti-Sca1 (1:100, BD Pharmingen) directly conjugated FITC or Cy3 anti-alpha-SMA (1:100–1:200, Sigma), and biotinylated anti-PDGFR-β (1:50–100, R&D). Secondary antibodies were conjugated to either Alexa -488, −555, −647 (Molecular Probes) or Dylight 649 (Jackson Labs) fluorophores or to biotin (1:250). Note that mTomato fluorescence from the unrecombined *ROSA26R*^{mTmG} allele is weak in lung cryosections or methanol-treated whole mount lungs, and certainly insignificant compared to the signal from immunostains with the anti-alpha-SMA antibody directly conjugated to Cy3. To mark nuclei, tissue was stained with DAPI (1:1000).

The positions of PA wall cells were identified as located in layer 1 (L1; i.e. the cell layer adjacent to the ECs), 2 (L2; the next radial layer) or adventitia (A; the following outer layer). The identity of layer A as adventitia should be considered provisional because these cells did not detectably express stem cell antigen-1 or patched-lacZ, the extant adventitial markers that label adventitia of select regions of specific vessels starting late in embryogenesis (Majesky et al., 2011; Passman et al., 2008). For quantification of marker expression profiles in PA wall layers, longitudinal confocal sections and vascular wall cells in each section were assessed as described below for phosphohistone cell counts. L1 cells of each section were numbered sequentially around the vessel and subdivided into groups of five contiguous cells. One cell was randomly selected from each group, and the marker expression was determined for this L1 cell as well as for the adjacent cell in L2 and the successive adjacent cell in A.

In situ hybridization

Dehydrated whole mount lungs were rehydrated into PBS with 0.1% Tween-20, permeabilized with proteinase K (10 mg/ml) and fixed again in 4% PFA with 0.2% glutaraldehyde (Sigma). Lungs were then hybridized at 68°C with digoxigenin (DIG)-labeled (Roche) probes overnight, washed extensively in saline sodium citrate solution and incubated with alkaline phosphate-conjugated anti-DIG antibodies at 4°C overnight. Nitro blue tetrazolium chloride/5-bromo-4-chloro-3′-indolyphosphate p-toluidine salt (NBT-BCIP) was used to detect signal, and lungs were then washed extensively with TBS/0.1% Tween-20/10 mM EDTA. Tissue sections (10 – 20 μm) were hybridized and stained as described (Red-Horse et al., 2010).

Phosphohistone cell counts and mitotic axis

Whole mount lungs stained with antibodies against pH3, SMA, and PDGFR-β and with DAPI were imaged by confocal fluorescence microscopy in the coronal plane to obtain longitudinal optical sections of the left PA extending from the carina to the first left lateral secondary airway branch (LL1). The longitudinal section of the left PA closest to the carina was the starting section and subsequent sections were collected every 12 – 20 μm (~1 cell length) until the vessel crossed LL1. Sections were considered adequate for analysis if the lumen and at least four cell lengths in the longitudinal axis of the vessel wall were visible. Sections containing wall cells visualized on previous sections were omitted. Vascular wall cells were identified as located in L1, L2 or A. This analysis included cells on the medial or lateral aspect of the blood vessel wall but excluded cells at the proximal or distal end of each vessel section because the layer these cells reside in could not be reliably determined. Between the carina and the LL1 airway branch, the left PA curves dorsal-ventrally, precluding definitive assignment to a specific wall layer at the proximal or distal end of each coronal section of the vessel. For mitotic axis counts, cells were only included in the analysis if they were $pH3^+$ and the division axis of the mitotic figure was clearly determinable. The long axis of the PA endothelium was defined as the longitudinal axis, and mitotic angles were scored relative to this axis and binned into three groups: longitudinal, radial or 45°. However, no mitotic figures in the 45° group were observed. An analysis of pH3-stained mitotic figures co-stained for acetylated tubulin to show the mitotic spindle confirmed the fidelity of this approach for assigning axis of division.

Clonal analysis

*SMMHC-CreER^{T2}*mice were crossed to either *ROSA26R^{mTmG}* or *ROSA26R^{Rb}* (“Rainbow”) mice. A single limiting dose (0.8 – 1.2 mg, see below) of tamoxifen (Sigma) was injected intraperitoneally into dams at E11.5 to induce recombination. Embryos were allowed to continue development and then analyzed at E13.5–18.5. For mGFP labeled clones, whole mount lungs were dissected and stained with an anti-GFP antibody in whole mount preparations for E13.5–14.5 lungs, or in cryosections for E17.5–18.5 lungs. Each GFP^+ cell was counted and its specific location and layer in the left PA wall recorded, except for cells at the proximal or distal end of each vessel section, which as described above could only be assigned to a ventral or dorsal location but not a specific layer of the PA wall. For Rainbow clones, tissue was cryosectioned and imaged using fluorescent filters for each fluorophore, and each marked cell was scored for color (i.e., Cerulean, mOrange or mCherry), position, and specific layer of the PA wall.

To find conditions of very sparse and, ideally, single cell (i.e. clonal) marking of left PA SMCs we titrated down the dose of tamoxifen injected at E11.5 in preliminary experiments. In the range used here (0.8 – 1.2 mg), we found that ~half (48%) of *SMMHC-CreER^{T2}*, *ROSA26R$^{mTmG/+}$* embryos had marked cells in the PA and the rest had none. Lower doses (0.6 mg) gave no GFP^+ PA SMCs at E13.5 (n=6), whereas higher doses (1.5 mg) yielded more embryos (83%) with marked cells and more GFP^+ cells in the marked embryos. To help ensure clonal labeling, we excluded from analysis any embryos in which there was not at least one *SMMHC-CreER^{T2}*, *ROSA26R$^{mTmG/+}$* littermate lacking marked cells. At standard doses of tamoxifen (0.8 – 1.2 mg) in *SMMHC-CreER^{T2}, ROSA26R$^{Rb/+}$* embryos (n=63), the PA SMCs were almost always unlabeled (59%) or labeled with just a single color (38%), confirming clonality, and only very rarely (n=2) were multi-color (i.e., polyclonal; 3%).

In these experiments, the labeled parent cell is always an inner layer SMC because expression of SMC markers (and presumably SMMHC-$CreER^{T2}$) is limited to this layer until three days after tamoxifen injection (i.e., E14.5; see Figs. 2, S2), and analysis of clones

marked at E11.5 and analyzed at E13.5 showed labeling of only inner layer cells. In embryonic studies from other groups utilizing highly active promoters driving *CreER*, the time window for recombination of Cre reporters is 6 – 48 h following a single injection of high dose tamoxifen (1.5–3.0 mg) (Hayashi and McMahon, 2002; Nakamura et al., 2006). We found that injection of our standard dose of tamoxifen (1.2 mg) at E10.5, instead of E11.5, resulted in no marked left PA SMCs in *SMMHC-CreER^{T2}*, *ROSA26R$^{mTmG/+}$* embryos at E13.5 (n=8). Because SMMHC protein (and presumably SMMHC-CreER^{T2}) is expressed in the PA SMCs at E11.5 (Fig. S2F), these findings suggest that the outer time limit for recombination in the left PA following a 1.2 mg injection is one day or less. Although there were no marked PA SMCs in these experiments, there were marked airway SMCs because expression of SMC markers, presumably including SMMHC-CreER^{T2}, occurs earlier in the airways than in the vessels. Similarly for *SMMHC-CreER^{T2}*, *ROSA26R$^{Rb/+}$* embryos from dams injected with tamoxifen at E11.5, PA SMCs were almost always unlabeled or labeled with a single color, but airway SMCs invariably contained marked cells of all three colors (Fig. S3F).

Lung cultures and PDGF bead implantation

Agarose beads (Affi-Gel Blue Gel, 100–200 mesh, Bio-Rad) were washed with sterile PBS three times for 30 min each, and then incubated for one hour with a disulfide linked homodimer of PDGF-B (R&D, 200–300 ng/ml) in PBS or with PBS alone for control beads (Furuta et al., 1997). After incubation, the beads were briefly washed and then implanted in the mesenchyme of freshly harvested E12 whole mount lungs by making a small incision in the lung mesenchyme with flame-polished tungsten needles and carefully positioning the bead. Lungs were cultured in DMEM12 with 10% FBS on 0.4 μm filters (Millipore) at the air liquid interface for 24–72 h in a 5% CO2 incubator, then fixed with 4% PFA and immunostained as above. Lungs that did not grow normally in culture were excluded from analysis.

Imaging

Tissue samples were imaged on a Leica MZ12 stereomicroscope (whole mounts) or on Zeiss Axiophot or Nikon Eclipse 80i fluorescence microscopes or on Leica CTR6000 or Nikon Eclipse Ti – Perkin Elmer Ultraview VoX confocal microscopes. Adobe Photoshop was used to process images and overlays.

Supplementary Material

Refer to Web version on PubMed Central for supplementary material.

Acknowledgments

We thank Krasnow laboratory members for input, including G. Fish for help with *in situ* studies, P. Bogard for help generating the *Tbx4-Cre* and *Tbx4-CreER^{T2}* mice and M. Petersen for help preparing figures. We also thank R. Adams, C. Betsholtz, P. Soriano and I. Weissman for mouse strains. D.M.G. was supported by the Sarnoff Foundation for Cardiovascular Science, Pulmonary Hypertension Association, National Institute of Health under the K08 Award (5K08HL093362) and Stanford University School of Medicine Pediatric Research Fund. M.A.K. is an investigator of the Howard Hughes Medical Institute. This work was supported by the National Institutes of Health under the Progenitor Cell Biology Consortium Grant (5U01HL099995) and under the Vascularization and Lung Development Grant (5R01HL075769) that ended two years ago, and by the Vera M. Wall Center for Pulmonary Vascular Disease at Stanford School of Medicine to M.A.K.

References

Adams RH, Alitalo K. Molecular regulation of angiogenesis and lymphangiogenesis. Nat Rev Mol Cell Biol. 2007; 8:464–478. [PubMed: 17522591]

Andrae J, Gallini R, Betsholtz C. Role of platelet-derived growth factors in physiology and medicine. Genes Dev. 2008; 22:1276–1312. [PubMed: 18483217]

Carmeliet P. Angiogenesis in life, disease and medicine. Nature. 2005; 438:932–936. [PubMed: 16355210]

Chung IM, Schwartz SM, Murry CE. Clonal architecture of normal and atherosclerotic aorta: implications for atherogenesis and vascular development. Am J Pathol. 1998; 152:913–923. [PubMed: 9546352]

DeRuiter MC, Poelmann RE, VanMunsteren JC, Mironov V, Markwald RR, Gittenberger-de Groot AC. Embryonic endothelial cells transdifferentiate into mesenchymal cells expressing smooth muscle actins in vivo and in vitro. Circ Res. 1997; 80:444–451. [PubMed: 9118474]

Domenga V, Fardoux P, Lacombe P, Monet M, Maciazek J, Krebs LT, Klonjkowski B, Berrou E, Mericskay M, Li Z, et al. Notch3 is required for arterial identity and maturation of vascular smooth muscle cells. Genes Dev. 2004; 18:2730–2735. [PubMed: 15545631]

Esner M, Meilhac SM, Relaix F, Nicolas JF, Cossu G, Buckingham ME. Smooth muscle of the dorsal aorta shares a common clonal origin with skeletal muscle of the myotome. Development. 2006; 133:737–749. [PubMed: 16436625]

Feng X, Krebs LT, Gridley T. Patent ductus arteriosus in mice with smooth muscle-specific Jag1 deletion. Development. 2010; 137:4191–4199. [PubMed: 21068062]

Foo SS, Turner CJ, Adams S, Compagni A, Aubyn D, Kogata N, Lindblom P, Shani M, Zicha D, Adams RH. Ephrin-B2 controls cell motility and adhesion during blood-vessel-wall assembly. Cell. 2006; 124:161–173. [PubMed: 16413489]

Frid MG, Dempsey EC, Durmowicz AG, Stenmark KR. Smooth muscle cell heterogeneity in pulmonary and systemic vessels. Importance in vascular disease. Arterioscler Thromb Vasc Biol. 1997; 17:1203–1209. [PubMed: 9261247]

Frid MG, Moiseeva EP, Stenmark KR. Multiple phenotypically distinct smooth muscle cell populations exist in the adult and developing bovine pulmonary arterial media in vivo. Circ Res. 1994; 75:669–681. [PubMed: 7923613]

Furuta Y, Piston DW, Hogan BL. Bone morphogenetic proteins (BMPs) as regulators of dorsal forebrain development. Development. 1997; 124:2203–2212. [PubMed: 9187146]

Gaengel K, Genove G, Armulik A, Betsholtz C. Endothelial-mural cell signaling in vascular development and angiogenesis. Arterioscler Thromb Vasc Biol. 2009; 29:630–638. [PubMed: 19164813]

Greif, DM. Vascular embryology and angiogenesis. In: Creager, M.; Beckman, J.; Loscalzo, J., editors. Vascular Medicine, A Companion to Braunwald's Heart Disease. New York: Elsevier; (in press)

Hamilton TG, Klinghoffer RA, Corrin PD, Soriano P. Evolutionary divergence of platelet-derived growth factor alpha receptor signaling mechanisms. Mol Cell Biol. 2003; 23:4013–4025. [PubMed: 12748302]

Hayashi S, McMahon AP. Efficient recombination in diverse tissues by a tamoxifen-inducible form of Cre: a tool for temporally regulated gene activation/inactivation in the mouse. Dev Biol. 2002; 244:305–318. [PubMed: 11944939]

High FA, Zhang M, Proweller A, Tu L, Parmacek MS, Pear WS, Epstein JA. An essential role for Notch in neural crest during cardiovascular development and smooth muscle differentiation. J Clin Invest. 2007; 117:353–363. [PubMed: 17273555]

Hirschi KK, Rohovsky SA, D'Amore PA. PDGF, TGF-beta, and heterotypic cell-cell interactions mediate endothelial cell-induced recruitment of 10T1/2 cells and their differentiation to a smooth muscle fate. J Cell Biol. 1998; 141:805–814. [PubMed: 9566978]

Hoch RV, Soriano P. Roles of PDGF in animal development. Development. 2003; 130:4769–4784. [PubMed: 12952899]

Hoglund VJ, Majesky MW. Patterning the artery wall by lateral induction of notch signaling. Circulation. 2012; 125:212–215. [PubMed: 22147908]

Hungerford JE, Little CD. Developmental biology of the vascular smooth muscle cell: building a multilayered vessel wall. J Vasc Res. 1999; 36:2–27. [PubMed: 10050070]

Hungerford JE, Owens GK, Argraves WS, Little CD. Development of the aortic vessel wall as defined by vascular smooth muscle and extracellular matrix markers. Dev Biol. 1996; 178:375–392. [PubMed: 8812136]

Jiang X, Rowitch DH, Soriano P, McMahon AP, Sucov HM. Fate of the mammalian cardiac neural crest. Development. 2000; 127:1607–1616. [PubMed: 10725237]

Jin SW, Beis D, Mitchell T, Chen JN, Stainier DY. Cellular and molecular analyses of vascular tube and lumen formation in zebrafish. Development. 2005; 132:5199–5209. [PubMed: 16251212]

Kirby ML, Gale TF, Stewart DE. Neural crest cells contribute to normal aorticopulmonary septation. Science. 1983; 220:1059–1061. [PubMed: 6844926]

Le Lievre CS, Le Douarin NM. Mesenchymal derivatives of the neural crest: analysis of chimaeric quail and chick embryos. J Embryol Exp Morphol. 1975; 34:125–154. [PubMed: 1185098]

Leveen P, Pekny M, Gebre-Medhin S, Swolin B, Larsson E, Betsholtz C. Mice deficient for PDGF B show renal, cardiovascular, and hematological abnormalities. Genes Dev. 1994; 8:1875–1887. [PubMed: 7958863]

Lindahl P, Johansson BR, Leveen P, Betsholtz C. Pericyte loss and microaneurysm formation in PDGF-B-deficient mice. Science. 1997; 277:242–245. [PubMed: 9211853]

Lindblom P, Gerhardt H, Liebner S, Abramsson A, Enge M, Hellstrom M, Backstrom G, Fredriksson S, Landegren U, Nystrom HC, et al. Endothelial PDGF-B retention is required for proper investment of pericytes in the microvessel wall. Genes Dev. 2003; 17:1835–1840. [PubMed: 12897053]

Majesky MW. Developmental basis of vascular smooth muscle diversity. Arterioscler Thromb Vasc Biol. 2007; 27:1248–1258. [PubMed: 17379839]

Majesky MW, Dong XR, Hoglund V, Mahoney WM Jr, Daum G. The adventitia: a dynamic interface containing resident progenitor cells. Arterioscler Thromb Vasc Biol. 2011; 31:1530–1539. [PubMed: 21677296]

Manderfield LJ, High FA, Engleka KA, Liu F, Li L, Rentschler S, Epstein JA. Notch activation of Jagged1 contributes to the assembly of the arterial wall. Circulation. 2012; 125:314–323. [PubMed: 22147907]

McLean SE, Mecham BH, Kelleher CM, Mariani TJ, Mecham RP. Extracellular matrix gene expression in the developing mouse aorta. Advances in Developmental Biology. 2005; 15:81–128.

Menke DB, Guenther C, Kingsley DM. Dual hindlimb control elements in the Tbx4 gene and region-specific control of bone size in vertebrate limbs. Development. 2008; 135:2543–2553. [PubMed: 18579682]

Metzger RJ, Klein OD, Martin GR, Krasnow MA. The branching programme of mouse lung development. Nature. 2008; 453:745–750. [PubMed: 18463632]

Miano JM, Cserjesi P, Ligon KL, Periasamy M, Olson EN. Smooth muscle myosin heavy chain exclusively marks the smooth muscle lineage during mouse embryogenesis. Circ Res. 1994; 75:803–812. [PubMed: 7923625]

Mizugishi K, Yamashita T, Olivera A, Miller GF, Spiegel S, Proia RL. Essential role for sphingosine kinases in neural and vascular development. Mol Cell Biol. 2005; 25:11113–11121. [PubMed: 16314531]

Morimoto M, Liu Z, Cheng HT, Winters N, Bader D, Kopan R. Canonical Notch signaling in the developing lung is required for determination of arterial smooth muscle cells and selection of Clara versus ciliated cell fate. J Cell Sci. 2010; 123:213–224. [PubMed: 20048339]

Nakamura E, Nguyen MT, Mackem S. Kinetics of tamoxifen-regulated Cre activity in mice using a cartilage-specific CreER(T) to assay temporal activity windows along the proximodistal limb skeleton. Dev Dyn. 2006; 235:2603–2612. [PubMed: 16894608]

Nystrom HC, Lindblom P, Wickman A, Andersson I, Norlin J, Faldt J, Lindahl P, Skott O, Bjarnegard M, Fitzgerald SM, et al. Platelet-derived growth factor B retention is essential for development of normal structure and function of conduit vessels and capillaries. Cardiovasc Res. 2006; 71:557–565. [PubMed: 16831408]

Olson LE, Soriano P. PDGFRbeta signaling regulates mural cell plasticity and inhibits fat development. Dev Cell. 2011; 20:815–826. [PubMed: 21664579]

Owens GK, Kumar MS, Wamhoff BR. Molecular regulation of vascular smooth muscle cell differentiation in development and disease. Physiol Rev. 2004; 84:767–801. [PubMed: 15269336]

Parera MC, van Dooren M, van Kempen M, de Krijger R, Grosveld F, Tibboel D, Rottier R. Distal angiogenesis: a new concept for lung vascular morphogenesis. Am J Physiol Lung Cell Mol Physiol. 2005; 288:L141–149. [PubMed: 15377499]

Passman JN, Dong XR, Wu SP, Maguire CT, Hogan KA, Bautch VL, Majesky MW. A sonic hedgehog signaling domain in the arterial adventitia supports resident Sca1+ smooth muscle progenitor cells. Proc Natl Acad Sci U S A. 2008; 105:9349–9354. [PubMed: 18591670]

Phng LK, Gerhardt H. Angiogenesis: a team effort coordinated by notch. Dev Cell. 2009; 16:196–208. [PubMed: 19217422]

Que J, Wilm B, Hasegawa H, Wang F, Bader D, Hogan BL. Mesothelium contributes to vascular smooth muscle and mesenchyme during lung development. Proc Natl Acad Sci U S A. 2008; 105:16626–16630. [PubMed: 18922767]

Red-Horse K, Ueno H, Weissman IL, Krasnow MA. Coronary arteries form by developmental reprogramming of venous cells. Nature. 2010; 464:549–553. [PubMed: 20336138]

Schwartz SM. Smooth muscle migration in vascular development and pathogenesis. Transpl Immunol. 1997; 5:255–260. [PubMed: 9504144]

Schwartz SM, Murry CE. Proliferation and the monoclonal origins of atherosclerotic lesions. Annu Rev Med. 1998; 49:437–460. [PubMed: 9509274]

Soriano P. Abnormal kidney development and hematological disorders in PDGF beta-receptor mutant mice. Genes Dev. 1994; 8:1888–1896. [PubMed: 7958864]

Strilic B, Kucera T, Eglinger J, Hughes MR, McNagny KM, Tsukita S, Dejana E, Ferrara N, Lammert E. The molecular basis of vascular lumen formation in the developing mouse aorta. Dev Cell. 2009; 17:505–515. [PubMed: 19853564]

Suri C, Jones PF, Patan S, Bartunkova S, Maisonpierre PC, Davis S, Sato TN, Yancopoulos GD. Requisite role of angiopoietin-1, a ligand for the TIE2 receptor, during embryonic angiogenesis. Cell. 1996; 87:1171–1180. [PubMed: 8980224]

Wasteson P, Johansson BR, Jukkola T, Breuer S, Akyurek LM, Partanen J, Lindahl P. Developmental origin of smooth muscle cells in the descending aorta in mice. Development. 2008; 135:1823–1832. [PubMed: 18417617]

Weinstein BM, Lawson ND. Arteries, veins, Notch, and VEGF. Cold Spring Harb Symp Quant Biol. 2002; 67:155–162. [PubMed: 12858536]

Wilm B, Ipenberg A, Hastie ND, Burch JB, Bader DM. The serosal mesothelium is a major source of smooth muscle cells of the gut vasculature. Development. 2005; 132:5317–5328. [PubMed: 16284122]

Wirth A, Benyo Z, Lukasova M, Leutgeb B, Wettschureck N, Gorbey S, Orsy P, Horvath B, Maser-Gluth C, Greiner E, et al. G12-G13-LARG-mediated signaling in vascular smooth muscle is required for salt-induced hypertension. Nat Med. 2008; 14:64–68. [PubMed: 18084302]

Wolinsky H, Glagov S. A lamellar unit of aortic medial structure and function in mammals. Circ Res. 1967; 20:99–111. [PubMed: 4959753]

Yamashita J, Itoh H, Hirashima M, Ogawa M, Nishikawa S, Yurugi T, Naito M, Nakao K, Nishikawa S. Flk1-positive cells derived from embryonic stem cells serve as vascular progenitors. Nature. 2000; 408:92–96. [PubMed: 11081514]

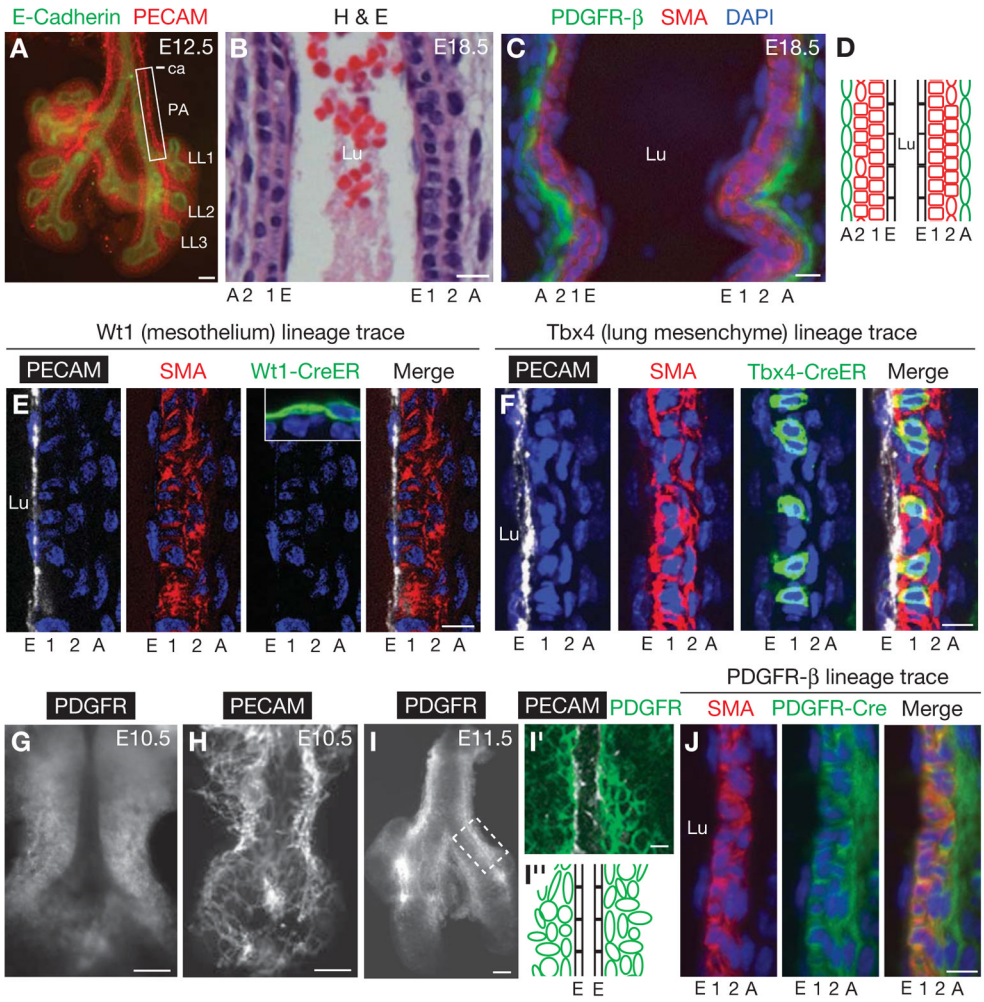

Figure 1. Pulmonary artery smooth muscle cells derive from lung mesenchyme

A, Ventral view of whole mount lung at embryonic day (E) 12.5 immunostained for E-cadherin (airway epithelium, green) and PECAM (endothelium, red). Box, portion of left pulmonary artery (PA) investigated here, from carina (ca) to LL1 (first lateral secondary branch off left primary bronchus) (Metzger et al., 2008). LL2 and LL3, second and third lateral secondary branches. **B, C,** Longitudinal sections of left PA at E18.5 stained with haematoxylin and eosin (H&E) (B) or immunostained for α-smooth muscle actin (SMA, red), PDGFR-β (green) and counterstained with DAPI (nuclei, blue) (C). E, endothelial cell (EC) layer; 1, first (inner) smooth muscle cell (SMC) layer; 2, second SMC layer; A, adventitial cell layer. Lu, PA lumen. **D**, Schematic of B and C, showing ECs (black), SMCs (red) and adventitial cells (green). **E, F,** Lineage tracing using the *Wt1-CreER*^{T2} and the *Tbx4-CreER*^{T2} transgenes as indicated with the mTmG Cre reporter to determine the contribution of the mesothelium and lung mesenchyme, respectively, to the PA wall. Longitudinal sections are shown of one side of the E18.5 left PA wall stained for the Cre reporter (green) and PECAM (white), SMA (red), and DAPI (blue) to visualize the PA wall. Pregnant dams were injected with a single dose of tamoxifen (3 mg at E9.5 in E; 1.5 mg at E10.5 in F) to activate the Cre(ER) recombinase. Inset in **E**, shows in the same specimen lineage-labeled cells in the lung mesothelium, outside the PA. Lineage trace of lung mesenchyme (F; also see Fig. S1C), but not mesothelium (E), labels PA wall cells, and the fraction of lineage labeled PA wall cells with the Tbx4-CreER^{T2} in F is similar to the overall

lung mesenchyme labeling efficiency (data not shown). **G**–**I**, PDGFR-β expression around developing PA. Whole mount lungs at indicated ages immunostained for PDGFR-β (G, I) and PECAM (endothelium, H). **I′**, Confocal optical section of boxed region of left PA in I showing both PDGFR-β and PECAM staining. **I″,** Schematic of I′ showing zone of PDGFR-β (green) cells surrounding developing left PA ECs (black). **J**, Lineage trace (as in E, F) of PDGFR-β expressing cells. All cells of E18.5 PA wall are marked by lineage tag (green). Scale bars, 100 μm **(A, G–I)** and 10 μm **(B, C, E, F, I′, J)**. (See also Figs. S1, S2A, C, D.)

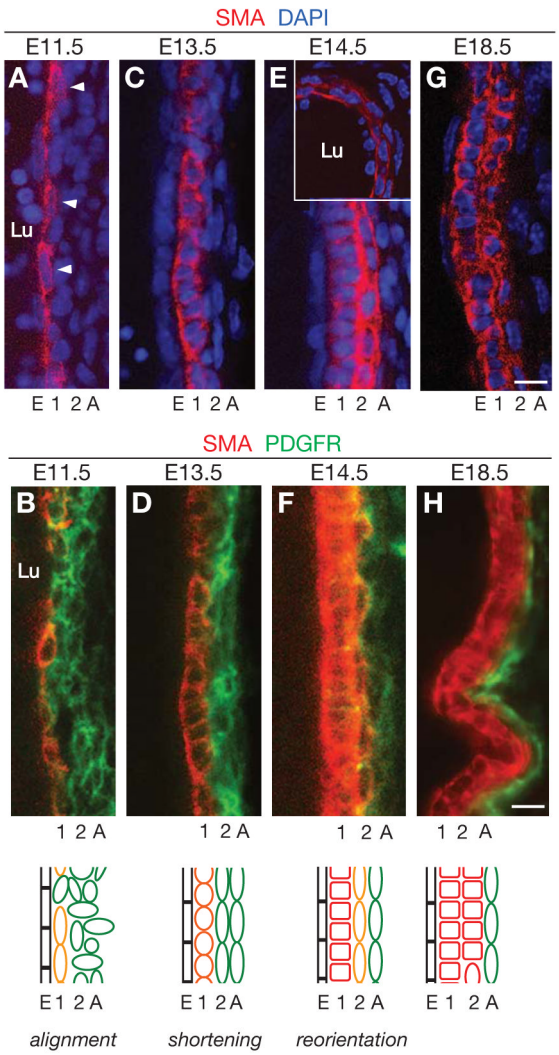

Figure 2. Radial development of the PA wall

Longitudinal sections through the left PA wall at the embryonic ages indicated, stained for SMA (red), PDGFR-β (green), and nuclei (DAPI, blue) as indicated. Arrowheads, nuclei elongated longitudinally. The inset in **E** shows a transverse section through the left PA wall. Schematics at bottom summarize SMA (red) and PDGFR-β (green) expression (orange, co-expression of SMA and PDGFR-β) and cell shape and orientation changes in the forming layers (E, 1, 2, A) of the developing PA wall. Lu, PA lumen. Square cells, circumferentially-oriented cells. Scale bars, 10 μm. (See also Fig. S2.)

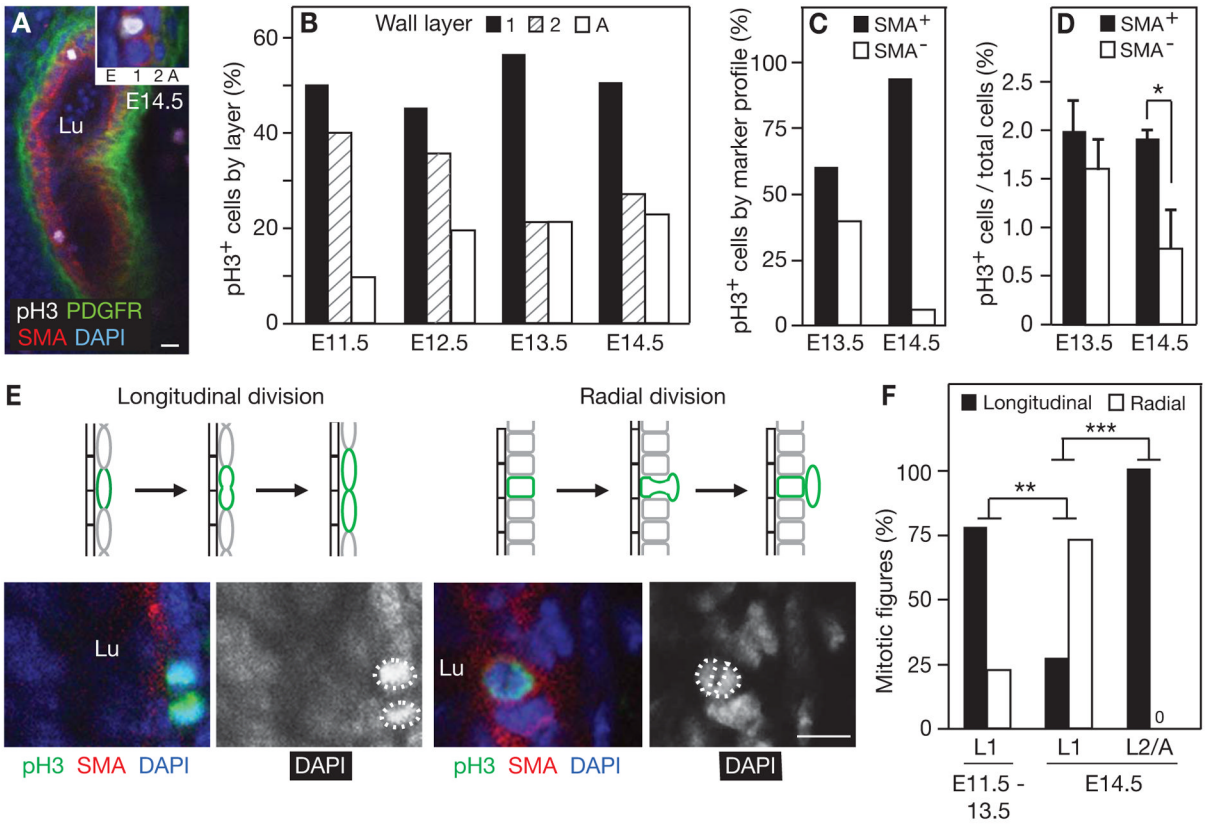

Figure 3. Radial patterning of cell division in the developing PA wall

A, Representative confocal optical section of left PA at E14.5 stained for the mitosis marker phosphohistone H3 (pH3, white) and SMA (red), PDGFR-β (green) and nuclei (DAPI, blue) to assign cell layer (1, 2, A) of each dividing cell. The inset shows a close up of a dividing cell and its assigned cell layer. **B,** Distribution of dividing cells among the three cell layers. Values shown are the fraction of all dividing ($pH3^+$) left PA wall cells located in each cell layer, for each embryonic age indicated. The total number of PA walls analyzed and dividing cells scored were: E11.5 (16 walls, 32 dividing cells), E12.5 (12, 31), E13.5 (14, 37) and E14.5 (15, 70). **C,** Marker expression pattern of dividing PA wall cells. Values shown are the fraction of all proliferating ($pH3^+$) left PA wall cells that were SMA^+ or PDGFR-β^+/SMA^-. The number of PA walls analyzed and dividing cells scored were: E13.5 (18, 48) and E14.5 (16, 80). **D,** Proliferative index of PA wall cells. Values shown are the proliferative index (fraction $pH3^+$ cells) of SMA^+ cells and PDGFR-β^+/SMA^- cells of the PA wall at the ages indicated. The number of left PA walls analyzed and cells scored were: E13.5 (18 walls, 1286 SMA^+ cells, 1111 PDGFR-β^+/SMA^- cells) and E14.5 (16, 3024, 519). Errors bars, s.e.m. *p=0.019 by Student's *t*-test. **E,** Schematic (top) and representative confocal images of stained lungs (bottom) showing longitudinal and radial axes of cell division in developing PA wall. Lungs were stained for pH3, SMA, and DAPI as indicated. Dashed circles, daughter chromosomes of dividing cell. **F,** Fraction of longitudinal vs. radial cell divisions in the indicated layers of the PA wall at the indicated ages. After E13.5, layer 1 (L1) cells switch from predominantly longitudinal to predominantly radial division. The "0" in the panel indicates no detected radial cell divisions in the L2 and A layers at E14.5. The number of mitotic figures scored at E11.5–13.5 was 22 in L1 and at E14.5 was 15 in L1 and 12 in L2 and A. **p=0.003, ***p=0.0002 by Fisher's exact test. Scale bars, 10 μm.

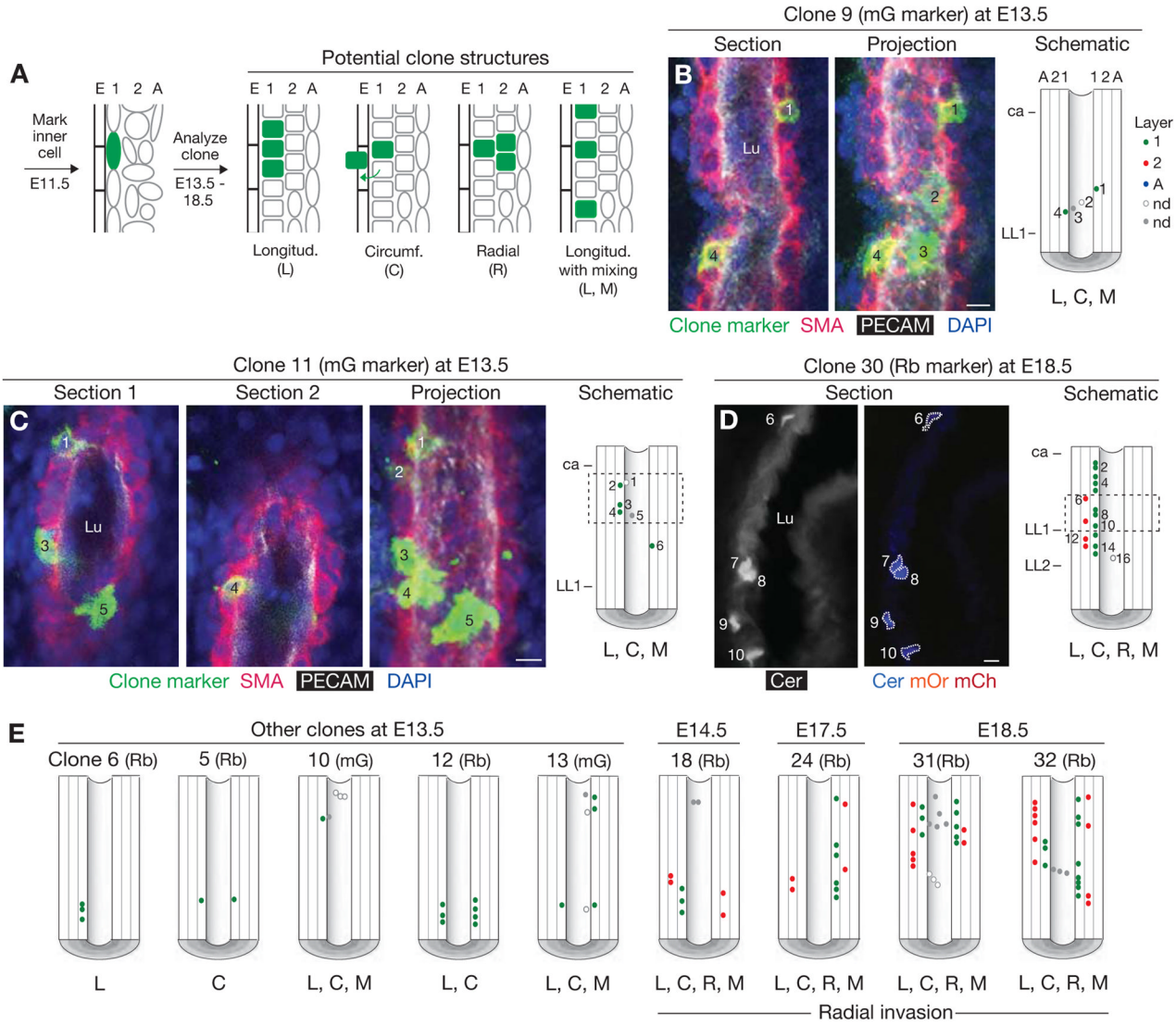

Figure 4. Clonal analysis of inner layer cells of the PA wall

A, Clonal analysis scheme showing early (E11.5) marking of an inner layer cell and four possible patterns of its proliferation and migration: longitudinal (L), circumferential (C), and radial (R) expansion, and longitudinal with mixing with unlabeled cells (L, M). **B,** A GFP-marked left PA clone (#9, Table S1) in a *SMMHC-CreER^{T2}, Rosa26R$^{mTmG/+}$* embryo, induced by administration of a limiting dose of tamoxifen at E11.5 and analyzed at E13.5 after staining for clone marker (membrane-localized GFP, abbreviated “mG”, green) and for SMA (red), PECAM (white) and nuclei (DAPI, blue). An individual coronal confocal optical section (dorsal view, anterior up) of the four-cell clone is shown (left panel) along with a maximal projection (center panel). 1–4, cells of clone; Lu, PA lumen. In the clone schematic (right panel), the positions of marked cells are indicated by circles color coded to highlight the layer in which the cell resides: green (layer 1), red (layer 2), and blue (adventitia). For cells located superficial (white circles) or deep (grey circles) to the lumen, we were unable to determine which layer they reside in (nd, not determined). This clone expanded longitudinally (L) and circumferentially (C), with mixing (M). ca, position of carina; LL1, position of LL1 airway branch. **C,** Six cell clone (#11), induced and analyzed as in B. Two confocal optical sections are shown, along with a maximal projection and

schematic. Dashed box, portion of clone shown in the confocal images. **D,** Sixteen cell clone (#30), induced and analyzed as in B, except clone marker was multicolor (Rainbow, abbreviated "Rb") ROSA26R^{Rb} Cre reporter and the clone was analyzed at E18.5. Left panel, Cerulean channel of confocal image (ventral view) of coronal cryosection of the clone: bright cells are Cerulean-expressing cells of clone (numbered). Faint background staining shows the rest of the SMCs of PA wall. Center panel, Cerulean, mOrange and mCherry channels of the same cryosection. All labeled cells in left PA express Cerulean marker, confirming clonality. Clone expanded in all three axes (L, C, and R), with some cells (red in schematic) having invaded layer 2. For clarity, only every other cell in the schematic is numbered. **E,** Schematics (ventral views) of other representative clones. Although layer 1 clones can expand and mix extensively within layer 1, they do not expand radially into layer 2 until E14.5. By E18.5, they have spread extensively in layers 1 and 2, but have not invaded the adventitial layer. mG, mGFP clone marker; Rb, Rainbow (multicolor) clone marker. Scale bars, 10 μm. (See also Table S1 and Figs. S3, S4.)

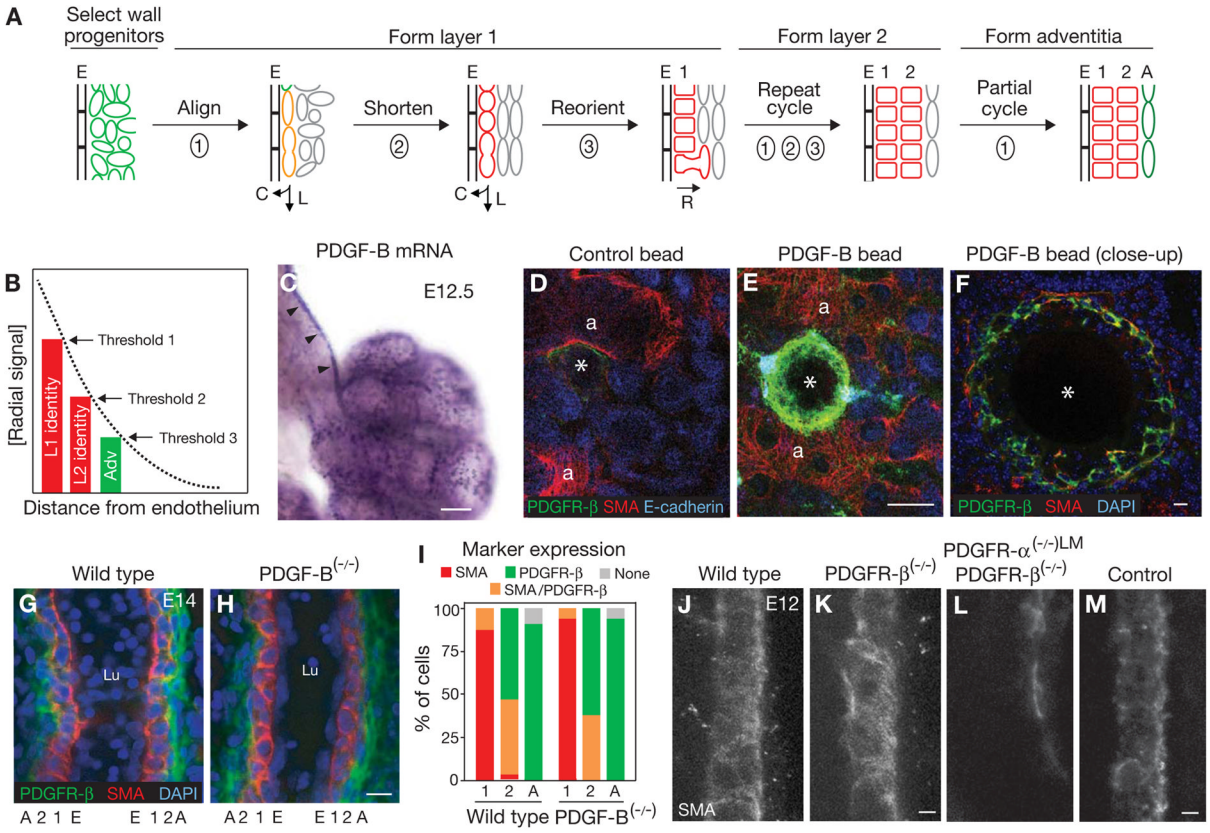

Figure 5. Signal gradient model for PA wall patterning and involvement of PDGF pathway

A, Summary of cellular and molecular events in radial construction of PA wall. Cell wall progenitor zone surrounding PA endothelial tube is initially marked by PDGFR-β expression (green cells). Innermost cells (adjacent to endothelium, E) initiate smooth muscle marker expression and morphogenesis (orange cells) and then down-regulate PDGFR-β (red cells) to form layer 1. Smooth muscle cycle repeats to form layer 2, and third cycle initiates to form adventitial (A) layer. As layer 1 cells mature, they radially reorient cell division and migration, sending daughter cells outward to supplement layer 2. R (radial), L (longitudinal), C (circumferential) cell division and migration. **B,** Gradient of a hypothetical radial signal that sequentially induces cell layers surrounding the endothelium to differentiate into the vascular wall. Different identity thresholds (1, 2, 3) result in differences among layers (e.g., smooth muscle vs. adventitia, or high vs. low elastin expression). The signaling gradient could also control the radial reorientation of cell division and migration. **C,** Whole mount lung *in situ* hybridization of the ligand PDGF-B, a candidate for the radial signal. Gene is expressed in ECs of developing PA (arrowheads). **D, E,** Confocal images of whole mount lungs from wild type littermates implanted with a control or PDGF-B-soaked bead as indicated, cultured for 72 hours and then stained for PDGFR-β (green), SMA (red), and E-cadherin (blue) and counterstained with DAPI (not shown). a, airway with associated smooth muscle; *, bead location. Phosphohistone H3 staining (not shown) did not demonstrate any obvious differences in cell division surrounding the beads. **F,** Close up of the region in **E** around the PDGF-B bead that has initiated arterial wall formation as shown by induction of PDGFR-β and SMA expression. **G–I,** Confocal optical sections of left PAs from whole mount E14 wild type (G) and *PDGF-B*$^{(-/-)}$ (H) littermate lungs stained for SMA, PDGFR-β and nuclei (DAPI) as indicated. Marker expression patterns are quantified in I, and values shown are fraction of cells in each layer with the indicated marker

expression profile. Three wild type PAs (n=96 cells) and two *PDGF-B*$^{(-/-)}$ PAs (48 cells) were scored. There is no detectable phenotype in the mutant. **J**–**M,** Confocal images of left PAs from whole mount E12 lungs of the indicated genotypes, immunostained for SMA. Because *PDGFR-α*$^{(-/-)}$, *PDGFR-β*$^{(-/-)}$ double mutants die before the PA wall forms, double mutant shown in **L** is a lung-mesenchyme-specific (LM) double knock-out of genotype *PDGFR-α*$^{(flox/-)}$, *PDGFR-β*$^{(-/-)}$, *Tbx4-Cre*. Airway branching, which is stereotypically correlated with PA development, is maintained in these mutants (data not shown). Genotype of littermate control in **M** is *PDGFR-α*$^{(flox/+)}$, *PDGFR-β*$^{(+/+)}$, *Tbx4-Cre*. Compound *PDGFR-α*$^{(+/-)}$, *PDGFR-β*$^{(-/-)}$ embryos at E11.5–12.5 did not show lung developmental delay or a PA phenotype (data not shown). Scale bars, 100 μm **(C, E)** and 10 μm **(F, H, K, M)**. (See also Fig. S5.)

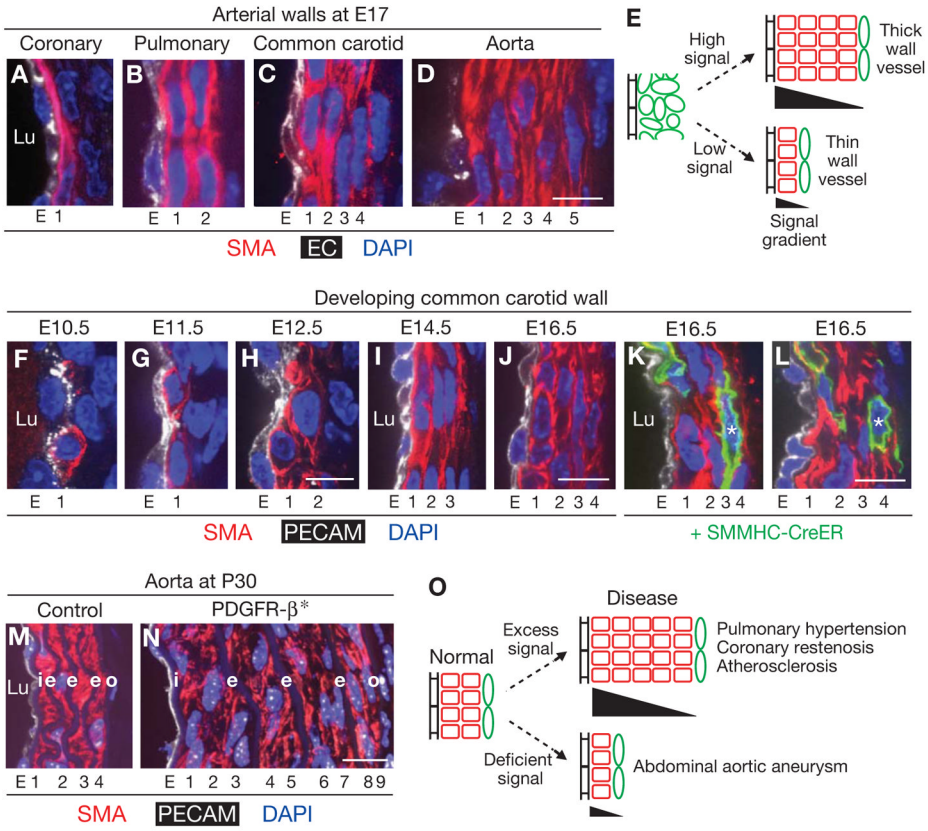

Figure 6. Radial patterning in arterial diversity and disease

A–D, Transverse sections of the left anterior descending coronary artery and the left pulmonary and left common carotid arteries (CCA) and aorta at ~E17, stained for SMA (red), EC marker (VE-cadherin in A and PECAM in B–D; white) and DAPI (nuclei, blue). Walls range from one to five smooth muscle layers thick. **E,** Differences in the radial signal gradient (see Fig. 5B) could determine the thickness of specific developing arteries. **F–J,** Sections through the developing left CCA (panel C) at the embryonic ages indicated and stained with SMA (red), PECAM (white) and DAPI (nuclei, blue). (Panels F-H are longitudinal sections of the third aortic arch artery, which later becomes the CCA, and panels I, J are transverse sections of the CCA.) Note the gradual increase in SMA^+ cell layers from rare first layer cells at E10.5 to four continuous circumferentially elongated layers at E16.5. **K, L,** Fate mapping of CCA first layer SMC $marker^+$ cells in *SMMHC-CreER^{T2}, Rosa26R$^{mTmG/+}$* embryos induced with a single low dose of tamoxifen (0.5mg) at E10.25. First layer CCA SMCs give rise to outer layer SMCs (marked by *), as for the PA (Figs. 4D, E, S4). Despite the different sizes and origins of the vascular wall cells (PA from mesenchyme, see Figs. 1F, J, S1C; CCA from neural crest, see ((Jiang et al., 2000; Le Lievre and Le Douarin, 1975)), radial invasion occurs in both vessels. **M, N,** Transverse sections of descending aortic walls stained for SMA, PECAM and nuclei (DAPI) in control(panel M, *SM22-Cre)* and a conditional PDGFR-β gain-of-function mutation activated specifically in smooth muscle (panel N, *PDGFR-β$^{(+/J)}$, SM22-Cre* indicated by PDGFR-β*). (The *PDGFR-β^J* allele, a V536A mutation that disrupts an inhibitory juxtamembrane region and results in constitutive PDGFR-β activity, isa knock-in at the endogenous *PDGFR-β* locus (Olson and Soriano, 2011)). Note that the mutant wall has more than twice the normal number of smooth muscle layers but the normal number of elastic layers (i, e, o) (N; Olson and Soriano, 2011), whereas in the PA there was no

observable phenotype (see Fig. S5D). **O,** Changes in the radial signaling gradient may contribute to diseases characterized by vessel wall thickening or thinning. E, endothelial layer; 1–9, smooth muscle layers 1–9; Lu, vessel lumen; i, internal elastic lamina; e, elastic lamina; o, external elastic lamina. Scale bars, 10 μm.